insufficient, suggesting that collective effects, such as velocity correlations between particles (*16*) or slowly decaying velocity autocorrelations, may be important.

All of the features in Fig. 3 refer to motions at times less than τ_c. At times longer than τ_c, the relative displacement of grains is characterized by subdiffusive motion, which presumably corresponds to gradual rearrangements of neighboring grains, over several orders of magnitude in time (Fig. 2, B and C). We did not obtain the diffusive limit $\langle \Delta r^2(\tau) \rangle \propto \tau$, even at the end of the range available to DWS. Measurements by long-range video microscopy (solid circles in Fig. 2C) show that relative motions of sand grains in the direction transverse to $V_f(\hat{y})$ and in the plane of the channel were diffusive (*17*). The time for rearrangement of nearest neighbors was 0.1 to 10 s, so that if relative motion is diffusive, it is a consequence of complex collective behavior. Hunt and others (*8*) reported experiments on video imaging of granular material in channel flow from which they extracted diffusion constants; similar experiments have been performed on vibrated granular systems (*9*). Our data indicate that the parameters of collisional dynamics cannot be deduced from such measurements using conventional prescriptions such as the Langevin equation as a bridge between short-time ballistic motion and long-time diffusion; for example, the diffusion coefficient of the grains in our experiment was much less than $s\delta V$.

The wide separation of time scales between collisional dynamics and the long-time diffusive limit suggest that complex collective dynamics occur even in the absence of long-wavelength clustering instabilities (*5*), reminiscent of dynamics in glassy systems such as viscous liquids and dense colloids. Our simple realization of a granular flow accentuates the contrast between a molecular fluid, where viscous loss occurs only in shear gradients, and sand, where a region of uniform flow dissipates energy because, as our results show, velocity fluctuations exist even in the absence of macroscopic gradients.

REFERENCES AND NOTES

1. H. M. Jaeger and S. R. Nagel, *Science* **255**, 1523 (1992); _____ and R. P. Behringer, *Phys. Today* **49**, 32 (April 1996); C. S. Campbell, *Annu. Rev. Fluid Mech.* **22**, 57 (1990).
2. R. A. Bagnold, *Proc. R. Soc. London Ser. A* **225**, 49 (1954); *ibid.* **295**, 219 (1966).
3. S. Ogawa, in *Proceedings of the U.S.–Japan Symposium on Continuum Mechanics and Statistical Approaches in the Mechanics of Granular Materials*, S. C. Cowin and M. Satake, Eds. (Gakujutsu Bunken Fukyukai, Tokyo, 1979), pp. 208–217; J. T. Jenkins and S. B. Savage, *J. Fluid Mech.* **130**, 187 (1983); P. K. Haff, *ibid.* **134**, 401 (1983); J. Schofield and I. Oppenheim, *Physica A* **196**, 209 (1993).
4. G. D. Cody, D. J. Goldfarb, G. V. Storch Jr., and A. N. Norris [*Powder Technol.* **87**, 211 (1996)] inferred velocity fluctuations in a fluidized bed from the acoustic response of the container to discrete collisions of particles.
5. M. A. Hopkins and M. Y. Louge, *Phys. Fluids A* **3**, 47 (1991); I. Goldhirsch and G. Zanetti, *Phys. Rev. Lett.* **70**, 1619 (1993); S. McNamara and W. Young, *Phys. Rev. E* **50**, R28 (1994); D. R. M. Williams and F. C. MacKintosh, *ibid.* **54**, R9 (1996).
6. G. Maret and P. E. Wolf, *Z. Phys. B* **65**, 409 (1987); D. J. Pine, D. A. Weitz, P. M. Chaikin, E. Herbolzheimer, *Phys. Rev. Lett.* **60**, 1134 (1988); D. J. Pine, D. A. Weitz, J. X. Zhu, E. Herbolzheimer, *J. Phys. (France)* **51**, 2101 (1990).
7. T. G. Drake, *J. Fluid Mech.* **225**, 121 (1991).
8. S. S. Hsiau and M. L. Hunt, *ibid.* **251**, 299 (1993); V. V. R. Natarajan, M. L. Hunt, E. D. Taylor, *ibid.* **304**, 1 (1995).
9. O. Zik and J. Stavans, *Europhys. Lett.* **16**, 255 (1991).
10. M. Nakagawa *et al.*, *Exp. Fluids* **16**, 54 (1993); E. E. Ehrichs *et al.*, *Science* **267**, 1632 (1995).
11. Jaygo (Union, NJ) and Cataphote (Jackson, MS).
12. The effect of the ambient air was small because the weight of the grains was at least 10^4 times the Stokes drag. Dissipation was primarily through inelastic collisions, which (for typical grain velocities and a coefficient of restitution of 0.9) was greater by a factor 10^4 than the energy lost to the viscous drag of the air.
13. S. Fraden and G. Maret, *Phys. Rev. Lett.* **65**, 512 (1990); X. Qiu *et al.*, *ibid.*, p. 516; J.-Z. Xue *et al.*, *ibid.* **69**, 1715 (1992).
14. O. Reynolds, *Philos. Mag.* **20**, 469 (1885).
15. K. Hui and P. K. Haff, *Int. J. Multiphase Flow* **12**, 189 (1986).
16. Y. H. Taguchi and H. Y. Takayasu, *Europhys. Lett.* **30**, 499 (1995).
17. These points are obtained from the width of $[\mathbf{r}(0) - \mathbf{r}(\tau)]\cdot\hat{\mathbf{y}}$ averaged over many particles and starting times. For comparison with the value of $\langle \Delta r^2(\tau) \rangle$ obtained from DWS, this quantity is multiplied by a factor of 3.
18. B. J. Berne and R. Pecora, *Dynamic Light Scattering: With Applications to Chemistry, Biology and Physics* (Wiley, New York, 1976).
19. We directly confirmed that the gradients in the other two directions were small by moving the beam across the channel.

5 August 1996; accepted 28 January 1997

Single-Electron Transport in Ropes of Carbon Nanotubes

Marc Bockrath, David H. Cobden, Paul L. McEuen,* Nasreen G. Chopra, A. Zettl, Andreas Thess, R. E. Smalley

The electrical properties of individual bundles, or "ropes," of single-walled carbon nanotubes have been measured. Below about 10 kelvin, the low-bias conductance was suppressed for voltages less than a few millivolts. In addition, dramatic peaks were observed in the conductance as a function of a gate voltage that modulated the number of electrons in the rope. These results are interpreted in terms of single-electron charging and resonant tunneling through the quantized energy levels of the nanotubes composing the rope.

In the past decade, transport measurements have emerged as a primary tool for exploring the properties of nanometer-scale structures. For example, studies of quantum dots have illustrated that single-electron charging and resonant tunneling through quantized energy levels regulate transport through small structures (*1*). Recently, much attention has been focused on carbon nanotubes (*2*). Their conducting properties are predicted to depend on the diameter and helicity of the tube, parameterized by a roll-up vector (n, m). One type of tube, the so-called (n, n) or armchair tube, is expected to be a one-dimensional (1D) conductor with current carried by a pair of 1D subbands (*3*) (Fig. 1, right inset). A recent breakthrough has made it possible to obtain large quantities of the (10, 10) single-walled nanotube (SWNT), which is ~1.4 nm in diameter (*4*). This advance, in combination with recent successes in performing electrical measurements on individual multiwalled nanotubes (MWNTs) (*5–7*) and nanotube bundles (*8*), makes possible the study of the electrical properties of this 1D system.

We have measured transport through bundles, or ropes, of nanotubes bridging contacts separated by 200 to 500 nm. A gap (suppressed conductance at low bias) is observed in the current-voltage (I-V) curves at low temperatures. Further, dramatic peaks are observed in the conductance as a function of a gate voltage V_g that modulates the charge per unit length of the tubes. These observations are consistent with single-electron transport through a segment of a single tube with a typical addition energy of ~10 meV and an average level spacing of ~3 meV.

The device geometry (Fig. 1, left inset) consists of a single nanotube rope to which

M. Bockrath, D. H. Cobden, P. L. McEuen, N. G. Chopra, A. Zettl, Molecular Design Institute, Lawrence Berkeley National Laboratory, and Department of Physics, University of California, Berkeley, CA 94720, USA.
A. Thess and R. E. Smalley, Center for Nanoscale Science and Technology, Rice Quantum Institute, and Departments of Chemistry and Physics, Mail Stop 100, Rice University, Post Office Box 1892, Houston, TX 77251, USA.
*To whom correspondence should be addressed.

lithographically defined leads have been attached. The tubes are fabricated as described in (4) and consist of ropes made up of ~1.4-nm-diameter SWNTs. Diffraction studies (9) indicate that ~30 to 40% of these are (10, 10) tubes. Contacts were made to individual ropes as follows. First, the nanotube material was ultrasonically dispersed in acetone and then dried onto an oxidized Si wafer on which alignment marks had previously been defined. An atomic force microscope (AFM) operating in the tapping mode was used to image the nanotubes. Once a suitable rope was found, its position was noted relative to the alignment marks. Resist was then spun over the sample, and electron beam lithography was used to define the lead geometry. Metal evaporation of 3 nm of Cr then 50 nm of Au followed by lift-off formed the leads. This device has four contacts and allows different segments of the rope to be measured and four-terminal measurements to be performed. The device was mounted on a standard chip carrier, contacts were wire bonded, and the device was loaded into a ^{4}He cryostat. A dc bias could be applied to the chip carrier base to which the sample was attached. This gate voltage V_g modified the charge density along the length of the rope. Four samples were studied at liquid helium temperatures. All of the data presented here, however, were obtained from a single 12-nm-diameter rope containing ~60 SWNTs.

Figure 1 shows the *I-V* characteristics of the nanotube rope section between contacts 2 and 3 as a function of temperature T. The conductance is strongly suppressed near $V = 0$ for $T < 10$ K. Gaps of a similar magnitude were obtained for other nanotube ropes with diameters varying from 7 to 12 nm and lengths from 200 to 500 nm. There was no clear trend in the size of the gap or the high-bias conductance with the rope length or diameter. We note that measurements of MWNTs by ourselves and others (5, 7) displayed no such gap in their *I-V* curves. These results are in rough agreement, however, with those reported previously by Fischer *et al.* (8) on similar, but longer, ropes of SWNTs. In their experiments, the linear-response conductance also decreased at low temperatures.

Remarkably, the linear-response conductance G of the rope segment as a function of V_g (Fig. 2A) consists of a series of sharp peaks separated by regions of very low conductance. The peak spacing varies significantly but is typically ~1.5 V. The peaks also vary widely in height, with the maximum amplitude of isolated peaks approaching e^2/h, where e is the electronic charge and h is Planck's constant. The peaks are reproducible, although sudden changes ("switching") in their positions sometimes occur, particularly at larger voltages. The peak width increases linearly with T (Fig. 2C), whereas the peak amplitude decreases (Fig. 2B). The most isolated peaks remain discernible even at $T = 50$ K.

The differential conductance dI/dV of a rope (Fig. 3) is reminiscent of previous measurements of Coulomb blockade (CB) transport in metal and semiconductor wires and dots (1). In these systems, transport occurs by tunneling through an isolated segment of the conductor or dot that is defined either by lithographic patterning or disorder. Tunneling on or off this dot is governed by the single-electron addition and excitation energies for this small system. The period of the peaks in gate voltage, ΔV_g, is determined by the energy for adding an additional electron to the dot. In the simplest model that takes into account both Coulomb interactions and energy-level quantization, which we refer to as the CB model, the peak spacing is given by

$$\Delta V_g = (U + \Delta E)/e\alpha \qquad (1)$$

where $U = e^2/C$ is the Coulomb charging energy for adding an electron to the dot, ΔE is the single-particle level spacing, and $\alpha = C_g/C$ is the rate at which the voltage applied to the back gate changes the electrostatic potential of the dot; here C is the total capacitance of the dot, and C_g is the capacitance between the dot and the back gate.

To understand the dependence on V and V_g in more detail, consider the energy-level diagrams in Fig. 4. They show a dot filled with N electrons, followed by a gap $U + \Delta E$ for adding the $(N + 1)$th electron. Above this, additional levels separated by ΔE are shown, which correspond to adding the $(N + 1)$th electron to one of the excited single-particle states of the dot. At a gate voltage corresponding to a CB peak, the energy of the lowest empty state aligns with the electrochemical potential in the leads,

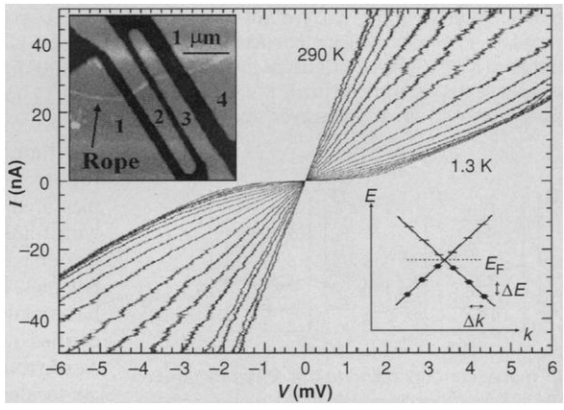

Fig. 1. The *I-V* characteristics at a series of different temperatures for the rope segment between contacts 2 and 3. (Left inset) AFM image of a completed device. The bright regions are the lithographically defined metallic contacts, labeled 1 to 4. The rope is clearly visible as a brighter stripe underneath the metallic contacts. Between the contacts (dark region), it is difficult to see the rope because of the image contrast. Note that the width of the rope in the AFM image reflects the convolution of its actual width with the AFM tip radius of curvature. The actual thickness of the rope is experimentally determined by measuring its height with the AFM and assuming that the rope is cylindrical. (Right inset) Schematic energy-level diagram of the two 1D subbands near one of the two Dirac points (3), with the quantized energy levels indicated. Here k points along the tube axis.

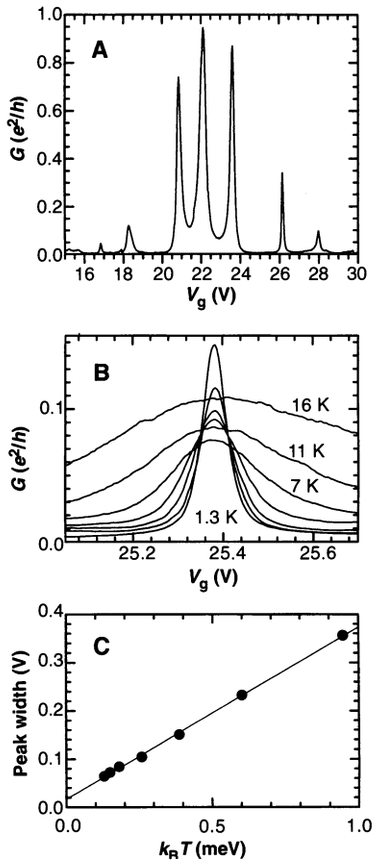

Fig. 2. (**A**) Conductance G versus gate voltage V_g at $T = 1.3$ K for the rope segment between contacts 2 and 3. (**B**) Temperature dependence of a peak. Note that this peak was measured on a run different from that in (A) and does not directly correspond to any of the peaks there. (**C**) Width of the peak in (B) as a function of T.

and single electrons can tunnel on and off the dot at $V = 0$ (Fig. 4A). At gate voltages in between peaks (Fig. 4B), tunneling is suppressed because of the single-electron charging energy U. However, if V is increased so that the electrochemical potential of the right lead is pulled below the energy of the highest filled state, an electron can tunnel off the dot, resulting in a peak in dI/dV (Fig. 4C). Further increasing V allows tunneling out of additional states, giving additional peaks in dI/dV (Fig. 4D). Similar processes occur for negative bias, corresponding to tunneling through unoccupied states above the Coulomb gap. At its largest, the required threshold voltage for the onset of conduction of either type is

$$V_{max} = U + \Delta E \quad (2)$$

To apply this model to our system, we must postulate that transport along the rope is dominated by single-electron charging of a small region of the rope, or perhaps a single tube within the rope. For now, we will use the CB model to infer the properties of this isolated region. We initially restrict ourselves to the data of Figs. 2 and 3, which corresponds to the rope segment between the two central contacts.

In the CB model, the temperature dependence can be used to deduce the parameters in Eq. 1. The width of a CB peak is given by $d(\Delta V_g)/dT = 3.5k_B/\alpha e$, where k_B is Boltzmann's constant. Comparison with the data in Fig. 2C gives $\alpha = 0.01$. From this value and the measured spacing between peaks of 1 to 2 V, we obtain a typical addition energy $U + \Delta E = 10$ to 20 meV. The disappearance of the oscillations above ~50 K yields a similar estimate for the addition energy.

The amplitude of the conductance peak increases with decreasing temperature at low temperatures. Within the extended CB model, this result indicates that $\Delta E \gg k_B T$ and that transport through the dot occurs by resonant tunneling though a single quantum level. The peak height decreases as T is increased up to ~10 K. This sets a lower bound on the energy-level splitting of $\Delta E \sim 1$ meV. In addition, for some peaks, such as those in the center of Fig. 2A, the intrinsic linewidths of the peaks are clearly observable. Fitting the peak shapes reveals that they are approximately Lorentzian, as expected for resonant tunneling through a single quantum level (*1*).

The nonlinear I-V measurements confirm the addition and excitation energies deduced above. The maximum size of the Coulomb gap V_{max} in Fig. 3 is a direct measure of the addition energy: for the two peaks in the figure, it is ~14 meV. Tunneling through excited states was also visible above the Coulomb gap for some peaks, and the level spacing to the first excited state ranged from 1 to 5 meV (*10*). For example, in Fig. 4 the level spacing between states labeled by C and D is $\Delta E = 1$ meV.

These parameters compare well with expectations. Consider a single (n, n) nanotube. The tube is predicted to be metallic (*3*), with two 1D subbands occupied at the Fermi energy E_F. The order of magnitude of the average level spacing should be related to the dispersion dE/dk ($\mathbf{k}$ is the wave vector) at the Fermi level (*3*, *11*)

$$\Delta E \sim \frac{dE}{dk}\frac{\Delta K}{2} \sim \frac{dE}{dk}\frac{\pi}{L} \sim \frac{0.5\ \text{eV}}{L\ (\text{nm})} \quad (3)$$

where the 2 arises from nondegeneracy of the two 1D subbands (Fig. 1, right inset). The charging energy is more difficult to estimate accurately. The actual capacitance of the dot depends on the presence of the leads, the dielectric constant of the substrate, and the detailed dielectric response of the rope (*12*). For an order of magnitude estimate, however, we take the capacitance to be given by the size of the object, $C = L$. We then have

$$U = \frac{e^2}{C} = \frac{e^2}{L} = \frac{14\ \text{eV}}{L\ (\text{nm})} \quad (4)$$

Note the remarkable result that in one dimension, both ΔE and U (Eqs. 3 and 4) scale as $1/L$, and hence the ratio of the charging energy to the level spacing is roughly independent of length. This independence means that the level spacing will be important even in fairly large dots, unlike in 3D systems. For a tube of length $L \sim 200$ nm (the spacing between the leads), we obtain $U = 7$ meV and $\Delta E = 2.5$ meV, consistent with the observed values.

To relate these theoretical results for a single tube to the measurements of rope samples, we first note that current in the rope is likely to flow along a filamentary pathway (*13*) consisting of a limited number of single tubes or segments of a few tubes each. This is because, first, 60 to 70% of the tubes are not (10, 10), and hence, the majority of the tubes in the rope will be insulating at low T (*14*). Second, the intertube conductance is small compared to the conductance along the tube, inhibiting intertube transport. Finally, the metal probably makes contact to only the metallic tubes on the surface of the rope, further limiting the number of tubes involved in transport.

Disorder along a filamentary pathway will tend to break it up into weakly coupled localized regions. This disorder may result from defects (*15*), twists (*16*), or places where intertube hopping is necessary along the pathway. Generally, the conductance should then be determined by single-electron charging and tunneling between a few such localized regions. For other rope segments that we have measured, the characteristics were consistent with transport through a few segments in series or parallel, each with different charging energies. For the particular rope segment we have focused on here, however, a single well-defined set of CB peaks was observed, indicating that transport was dominated by a single localized region. We believe that this region is a section of a single tube or possibly a bundle of a few tubes. The measured charging energies and level spacing indicate that the

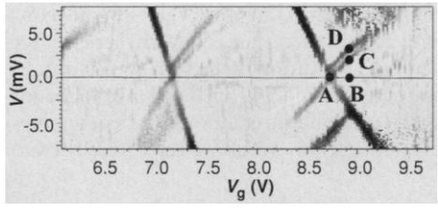

Fig. 3. Differential conductance dI/dV of the rope segment between contacts 2 and 3 as a function of V and V_g. The data are plotted as an inverted gray scale, with dark corresponding to large dI/dV. To enhance the image contrast, a smoothed version of the data was subtracted from the differential conductance. The points marked A through D correspond to the diagrams in Fig. 4. The linear-response conductance peaks (such as point A) correspond to the centers of the crosses along the horizontal line at $V = 0$. The gap in dI/dV corresponds to the white diamond-shaped regions between the crosses (such as the region containing point B). These crosses delineate the point of the onset of conduction at finite V (point C). Because the application of large biases led to significant switching of the device, our sweeps were limited to ±8 mV, and only the center of the diamond regions is visible. Additional features (point D) are also observed above the gap.

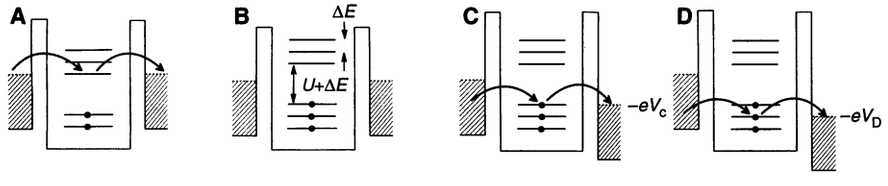

Fig. 4. Schematic energy-level diagrams within the CB model corresponding to the points marked on Fig. 3: (**A**) at a Coulomb peak, where linear-response ($V = 0$) transport is possible; (**B**) between peaks, where linear-response transport is blockaded (the addition energy $U + \Delta E$ and the level spacing ΔE are indicated here); (**C** and **D**) at two different applied voltages (V_C and V_D, the voltages at the respective points in Fig. 3), where transport occurs through the first and second occupied states, respectively.

size of this region is roughly the length between the contacts.

Each peak therefore corresponds to resonant tunneling though a coherent molecular state that extends for up to hundreds of nanometers in a localized region within the nanotube bundle. Furthermore, the amplitudes of some isolated peaks approach the theoretical maximum for single-electron transport of e^2/h. This amplitude is only possible if the barriers that confine this state at either end are approximately equal and there is no other significant resistance in series with the localized region. These requirements are consistent with the barriers being at the contacts between the metal leads and the rope. It is also possible that the barriers are within the rope, in which case the metal-rope contacts must be almost ideal so as not to reduce the maximum conductance from e^2/h (*17*). Variation in the coupling to each lead from level to level can account for the varying peak sizes apparent in Fig. 2.

Although the above interpretation accounts for the major features in the data, many interesting aspects of this system remain to be explored. First, one would like to establish absolutely that transport is indeed occurring predominantly along a single tube. Second, it should be determined whether all details of the data can be explained within the simple CB model discussed above, because Coulomb interactions may significantly modify the low-energy states from simple 1D noninteracting levels (*18*). Of great interest would be measurements of disorder-free tubes, where the intrinsic conducting properties of the tube can be measured without the complications of single-electron charging. To address these issues, experiments on individual single-walled tubes are highly desirable, and progress is being made in this direction (*19*). Yet another important experiment would be to measure directly the intertube coupling by making separate electrical contact to two adjacent tubes.

REFERENCES AND NOTES

1. For a review, see H. Grabert and M. H. Devoret, Eds., *Single Charge Tunneling* (Plenum, New York, 1991); M. A. Kastner, *Phys. Today* **46**, 24 (January 1993); L. P. Kouwenhoven and P. L. McEuen, in *Nanoscience and Technology*, G. Timp, Ed. (AIP Press, New York, in press).
2. S. Iijima, *Nature* **354**, 56 (1991); for a recent review, see T. W. Ebbesen, *Phys. Today* **49**, 26 (June 1996).
3. R. Saito, M. Fujita, G. Dresselhaus, M. S. Dresselhaus, *Appl. Phys. Lett.* **60**, 2204 (1992); N. Hamada, S. Sawada, A. Oshiyama, *Phys. Rev. Lett.* **68**, 1579 (1992).
4. A. Thess *et al.*, *Science* **273**, 483 (1996).
5. L. Langer *et al.*, *Phys. Rev. Lett.* **76**, 479 (1996).
6. H. Dai, E. W. Wong, C. M. Lieber, *Science* **272**, 523 (1996).
7. T. W. Ebbesen *et al.*, *Nature* **382**, 54 (1996); A. Yu. Kasumov, I. I. Khodos, P. M. Ajayan, C. Colliex, *Europhys. Lett.* **34**, 429 (1996).
8. J. E. Fischer *et al.*, *Phys. Rev. B* **55**, 4921 (1997).
9. D. Bernaerts *et al.*, preprint (1996); J. M. Cowley, P. Nikolaev, A. Thess, R. E. Smalley, *Chem. Phys. Lett.* **265**, 379 (1997).
10. The level spacing can be determined from the data in Fig. 3 by two means. The first means is to measure the separation between features in V_g and use the conversion factor $\alpha = V_{max}/\Delta V_g$. The second is to measure the separation between the features in V and use the slopes of the lines defining the Coulomb gap to infer $\alpha_L = C_L/C$ and $\alpha_R = C_R/C$. For more information, see (*1*).
11. H.-Y. Zhu, D. J. Klein, T. G. Schmalz, N. H. Rubio, N. H. March, preprint (1996).
12. L. X. Benedict, S. G. Louie, M. L. Cohen, *Phys. Rev. B* **52**, 8541 (1995).
13. Other measurements on these samples also support the notion that transport is through individual decoupled tubes. In four-terminal measurements of the ropes at temperatures > 30 K (where the rope resistance becomes much less than the voltage-probe impedance and reliable four-terminal measurements are possible), nonlocal voltages have been observed. For example, referring to the AFM image shown in Fig. 1, a voltage can appear between the terminals 1 and 2 in response to a current flowing between contacts 3 and 4. Such nonlocal effects are possible if different contacts make contact to different tubes and the intertube coupling is small. Current injected into 4 in a particular tube that is not well connected to 3 can arrive at contact 1 or 2, producing a nonlocal response.
14. Individual tubes within a rope have chiral angles within 10° of the achiral (10, 10) tube with roughly 30 to 40% of the sample being (10, 10) tubes (*9*). The indices of tubes consistent with the experimental constraints on chirality and radius (*4*) are (10, 10), (9, 11), (8, 12), (7, 13), and the opposite-handed twins. The gap of the (7, 13) tube is small and likely does not survive intertube interactions, but the gaps of the (9, 11) and (8, 12) tubes are about 0.5 eV, which is probably large enough to maintain semiconducting behavior within the rope.
15. L. Chico, L. X. Benedict, S. G. Louie, M. L. Cohen, *Phys. Rev. B* **54**, 2600 (1996); L. Chico *et al.*, *Phys. Rev. Lett.* **76**, 971 (1996).
16. C. L. Kane and E. J. Mele, *Phys. Rev. Lett.*, in press.
17. The large peak heights, combined with the fact that the room-temperature conductance of the center segment is also approximately e^2/h, imply that good electrical contact has been made between the metal leads and part of the rope.
18. Y. A. Krotov, D.-H. Lee, S. G. Louie, preprint (cond-mat/9611073, available on the Internet from the e-Print archive at xxx.lanl.gov); L. Balents and M. P. A. Fisher, preprint (cond-mat/9611126, available from the e-Print archive at xxx.lanl.gov).
19. S. Tans, preprint (1997).

20. We would like to acknowledge useful discussions with V. Crespi, M. Cohen, D. H. Lee, and S. Louie. We are also indebted to S. Tans for communicating his unpublished results of measurements on nanotubes and emphasizing the importance of a gate voltage. Supported by the U.S. Department of Energy, under contract DE-AC03-76SF00098, and by the Office of Naval Research, order N00014-95-F-0099.

13 December 1996; accepted 25 February 1997

Origin of the High-Frequency Doublet in the Vibrational Spectrum of Vitreous SiO_2

Johannes Sarnthein, Alfredo Pasquarello,* Roberto Car

The vibrational properties of amorphous SiO_2 were studied within first-principles density functional theory. The calculated spectrum is in good agreement with neutron data, showing, in particular, a double peak in the high-frequency region. This doublet results from different local modes of the tetrahedral subunits and cannot be ascribed to a longitudinal-optic–transverse-optic (LO-TO) effect. This solves a long-standing controversy about the origin of the doublet in neutron spectra. A LO-TO splitting is recovered only when the long-wavelength limit is probed, as in optical experiments. These findings should be a general feature of tetrahedral AX_2 amorphous networks.

The high-frequency vibrations in amorphous SiO_2 (a-SiO_2), corresponding to Si–O stretching modes, are responsible for a double peak that is clearly distinguishable in neutron spectra (*1*, *2*). In the same frequency range, infrared (*3*–*5*) and Raman measurements (*6*–*8*) show a LO-TO splitting induced by the long-range nature of the Coulomb fields that are present in ionic materials (*9*, *10*). Because the splittings in neutron and optical spectra are similar, two different explanations for their occurrence have been invoked. The splitting in the neutron spectrum has alternatively been attributed to two different vibrations of molecular subunits (*3*, *11*–*13*), with one of them being optically inactive, or interpreted as a LO-TO effect related to a single type of stretching mode (*14*, *15*).

The explanation in terms of a separation between LO and TO modes arises naturally as an extension from crystalline SiO_2. In α quartz, at the Γ point of the Brillouin zone, a splitting of about 20 meV between LO and TO phonon modes is indisputable (*16*, *17*). De Leeuw and Thorpe showed that the LO-TO splitting as observed in infrared spectra (that is, for a long-wavelength excitation) could be generalized to an amorphous system (*9*). However, their model failed to reproduce the double peak in the vibrational density of states that is observed with neutron scattering

J. Sarnthein, Institut Romand de Recherche Numérique en Physique des Matériaux (IRRMA), IN-Ecublens, CH-1015 Lausanne, Switzerland.
A. Pasquarello and R. Car, IRRMA, IN-Ecublens, CH-1015 Lausanne, Switzerland, and Department of Condensed Matter Physics, University of Geneva, CH-1211 Geneva, Switzerland.

*To whom correspondence should be addressed.